Full Engineering Laboratory Report

MAE 108 Aerospace Laboratory

Lab 4 Pressure Distribution Over an Airfoil and Hot-Wire Anemometry

Group Members:

Kevin Naraki Kim Wong (Group Leader)

Noah Palanjan (Primary Data Collector)

Matthew Valencia (Primary Data Collector)

Triet Ho (Analyst)

Yonghao Huo (Analyst)

Josue Guerrero (Technician)

Devrajsinh Mayurdhvajsinh Zala (Technician)

Vanessa Abigail Renderos

Tristan Reyes

Xuanqi Zang.

Advisers:

T.A. Cody Gonzalez

Prof. Sherif Hassaan

Date of Experiment: November 14, 2024

Submission Date: December 5, 2024

Table of Contents

Nomenclature List

SYMBOL	DEFINITION
C_p	Pressure coefficient (dimensionless)
D	Drag force (N)
h	Height of the body (m)
L	Lift Force (N)
M	Mach number (dimensionless)
p	Local static pressure (Pa)
p_∞	Freestream static pressure (Pa)
ρ	Density (kg/m^3)
S_{ref}	Reference area (m^2)
u	Velocity in the wake (m/s)
U_∞	Freestream velocity (m/s)
V	Velocity of the flow (m/s)
V_∞	Freestream velocity (m/s)

α	Angle of attack (degrees)
α'	Angle of attack (degrees)
C_D	Drag coefficient (dimensionless)
C_L	Lift coefficient (dimensionless)
C_M	Pitching moment coefficient (dimensionless)

List of Figures

List of Tables

1. Abstract

An experimental investigation was conducted to evaluate the aerodynamic performance of a Clark Y-14 airfoil using pressure distribution measurements and wake surveys. Pressure taps were distributed along the chord of the airfoil to measure the pressure distribution at various angles of attack (0°, 4°, 8°, and 20°). Lift and drag coefficients were computed from these pressure measurements. Additionally, an alternative drag coefficient was estimated to use wake momentum deficit measurements taken with a hot-wire anemometer. The results showed that the lift coefficient increased with the angle of attack, reaching a stall condition near 16°, where a sharp rise in the drag coefficient was observed. This investigation highlights the complementary nature of pressure and wake survey techniques for analyzing airfoil performance and underscores the importance of utilizing both methods to identify discrepancies between them. The findings demonstrate how these techniques can be used together to assess airfoil behavior more comprehensively.

2. Introduction

The study of airfoil aerodynamics is fundamental to optimizing the performance of aircraft and other aerodynamic structures. The Clark Y-14 airfoil, known for its flat-bottom design and maximum thickness of 14% of the chord length, serves as an ideal subject for experimental analysis due to its simplicity and well-documented behavior. Its unique characteristics, coupled with extensive historical data, make it a benchmark model for investigating fundamental aerodynamic properties such as lift and drag.

The aerodynamic performance of an airfoil is governed by the distribution of pressure across its surface, which depends on several factors, including the angle of attack, Reynolds number, and boundary layer characteristics. Accurate measurement of these aerodynamic forces involves various experimental techniques, each with its advantages. Pressure distribution measurements offer detailed insights into the local forces acting on the airfoil, while wake surveys allow for the indirect estimation of drag by analyzing momentum deficits downstream of the airfoil.

This study evaluates the aerodynamic performance of the Clark Y-14 airfoil at a range of angles of attack using pressure distribution data and wake momentum measurements. The

investigation examines both clean and modified configurations of the airfoil, including the addition of slats and flaps, to understand how these elements affect lift augmentation and stall characteristics. By comparing the results of both techniques, the study aims to explore the complementary nature of pressure and wake survey methods in analyzing airfoil performance.

The results from this experiment provide critical insights into the effects of slats and flaps on airfoil lift and drag, especially at high angles of attack. Understanding the interaction between these modifications and the aerodynamic forces acting on the airfoil is key to optimizing airfoil designs for various flight conditions. The report is structured as follows: the Background and Previous Work section reviews existing literature on airfoil performance and the methods used to measure lift and drag. The Theoretical Presentation provides the underlying aerodynamic theory and equations. The Experimental Procedure outlines the methodology used in the laboratory, followed by the Results section, which presents the data obtained from the experiments. Finally, the Conclusion section summarizes the outcomes and provides recommendations for future studies.

3. Background and previous work

The Clark Y-14 airfoil, introduced in the 1920s, has become a widely used benchmark for aerodynamic studies due to its straightforward geometry and predictable performance. Its design, featuring a flat lower surface and a maximum thickness of 14% of the chord length, makes it an ideal subject for investigating fundamental aerodynamic principles. Originally detailed in NACA Report No. 628, the Clark Y-14's performance has been extensively documented, making it a reference model in aerodynamic research.

Numerous methods have been developed to measure the aerodynamic characteristics of airfoils. Direct force measurement is one of the most straightforward approaches, involving the use of force balances or strain gauges to capture immediate data on lift and drag. However, this technique requires careful calibration and can be influenced by interference effects from the support structures.

Pressure integration, one of the earliest methods developed for wind tunnel testing, involves placing pressure taps along the airfoil surface to measure the pressure distribution. This technique provides valuable data on pressure drag, which results from flow separation and the

formation of vortices, and on friction drag, which is due to the viscous effects along the airfoil's surface. The precision of this method depends on the number and placement of the pressure taps, which are crucial for obtaining accurate results.

The wake survey method, pioneered by Jones in 1936 and refined by subsequent researchers, is a less intrusive technique for estimating drag [2]. By measuring the momentum deficit in the wake downstream of the airfoil, this method allows for drag determination without disturbing the flow. This technique has gained popularity for its ability to minimize interference while delivering reliable results for drag estimation.

The current experiment builds upon these established methods by applying both pressure distribution and wake survey techniques to the Clark Y-14 airfoil. It investigates how slats and flaps impact the aerodynamic performance of the airfoil at varying angles of attack, contributing to the broader understanding of lift, drag, and stall behavior.

4. Theoretical presentation

Aerodynamic analysis of an airfoil requires understanding of the fundamental concepts for both pressure-based and wake-based measurement techniques. This section presents the theoretical framework necessary for interpreting experimental results.

4.1. Pressure Distribution Analysis

The pressure field around an airfoil is critical for understanding the forces acting on it. The local pressure at any point on the airfoil surface can be expressed using the dimensionless pressure coefficient, C_p, defined as:

$$C_p = \frac{p - p_\infty}{\frac{1}{2}\rho V_\infty^2} \qquad \text{(Equation 4.1.1)}$$

where p is the local static pressure, p is the freestream static pressure, ρ is the air density, V_∞ is the freestream velocity. Negative values of C_p indicate regions of lower pressure, which are responsible for generating lift, while positive values correspond to regions of higher pressure, contributing to drag.

4.2. Force Calculation from Pressure Distribution

The aerodynamic force on the airfoil can be broken down into components normal and tangential to the chord line. These components are then transformed to calculate the lift and drag forces:

$$L = F_{p,N} cos\ \alpha - F_{p,c}\ sin\ \alpha \quad \text{(Equation 4.2.1)}$$

$$D = F_{p,c} cos\ \alpha + F_{p,N}\ sin\ \alpha \quad \text{(Equation 4.2.2)}$$

where $F_{p,N}$ is the normal component of the pressure force, $F_{p,c}$ is the parallel component to the chord, and α is the angle of attack.

4.3. Lift and Drag Coefficients

The lift coefficient C_L is a dimensionless measure of the lift force and is calculated using:

$$C_L = \frac{L}{\frac{1}{2}\rho V_\infty^2 S_{ref}} \quad \text{(Equation 4.3.1)}$$

where S_{ref} is the reference area of the airfoil, V_∞ is the freestream velocity, and ρ is the air density. Similarly, the drag coefficient C_D is calculated as:

$$C_D = \frac{D}{\frac{1}{2}\rho V_\infty^2 S_{ref}} \quad \text{(Equation 4.3.2)}$$

where D is the drag force

4.4 Wake Survey and Drag

The wake survey method uses the momentum deficit in the wake to estimate the drag force. Based on the principle of momentum conservation, the drag is calculated as:

$$D = \int_{-a}^{+a} h\rho U_\infty^2 dy - \int_{-b}^{+b} h\rho u^2 dy \quad \text{(Equation 4.4.1)}$$

where u is the velocity in the wake at a given point y, U_∞ is the freestream velocity, h is the height of the body, and ρ is the fluid density. This method provides an effective means of estimating drag with minimal disturbance to the flow.

5. Experimental procedure

The experiment involves three main procedures: hot-wire calibration, pressure force measurements, and wake measurements. The hot-wire anemometer is first calibrated to ensure accurate velocity measurements. Pressure force measurements are then taken at various angles of attack using pressure taps located along the airfoil. Finally, wake measurements are performed to estimate drag using the momentum deficit method.

5.1 Hot-wire calibration

a. Install the Pitot tube and connect it to the Setra Pressure Transducer to measure dynamic pressure.

b. Open the "NewMAE108Software.vi" LabVIEW program and turn the wind tunnel on to 5 m/s.

c. Load the "Hotwire experiment.vi" LabVIEW program and set the number of samples to 2000 and the sample rate to 500 Hz to collect data.

d. Record the dynamic pressure measurement and the anemometer voltage at various wind tunnel velocities (Channel 2).

e. Repeat step b, c, and d for wind tunnel velocities of 7, 9, 12, 15, 20, 25, 30, and 35 m/s.

f. Apply King's law to quantify the relationship between voltage and velocity using the collected data.

5.2 Pressure Force Measurements

a. Install the vertical airfoil model with the static pressure taps.

b. Connect the static pressure taps one-by-one to the high-pressure side of the pressure transducer, with the upstream static pressure connected to the low pressure side.

c. Operate the wind tunnel at 25 m/s and take pressure measurements at angles of attack of 0°, 4°, 8°, and 20°.

5.3 Wake Measurements

a. Set the wind tunnel velocity to 25 m/s using the Pitot tube.

b. Traverse the Pitot tube across the front of the airfoil to measure the inlet velocity profile.

c. Position the hot-wire anemometer at a known location behind the airfoil and record its position.

d. Switch the CTA to operate mode, set the number of samples to 5000 and collect 5 seconds of data at 1000 Hz.

e. Move the hot-wire probe to new locations and repeat the data collection to survey the wake.

f. Repeat step a through e for angles of attack of 4°, 8°, and 20°.

g. Turn off the CTA before turning off the wind tunnel.

6. Results

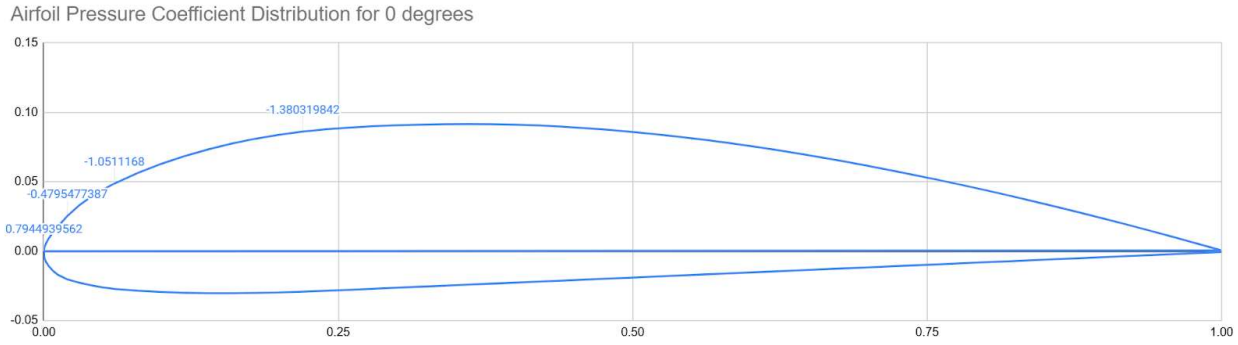

Figure 1: Pressure coefficient distribution of x-y locations on the airfoil surface for angle of attack 0°.

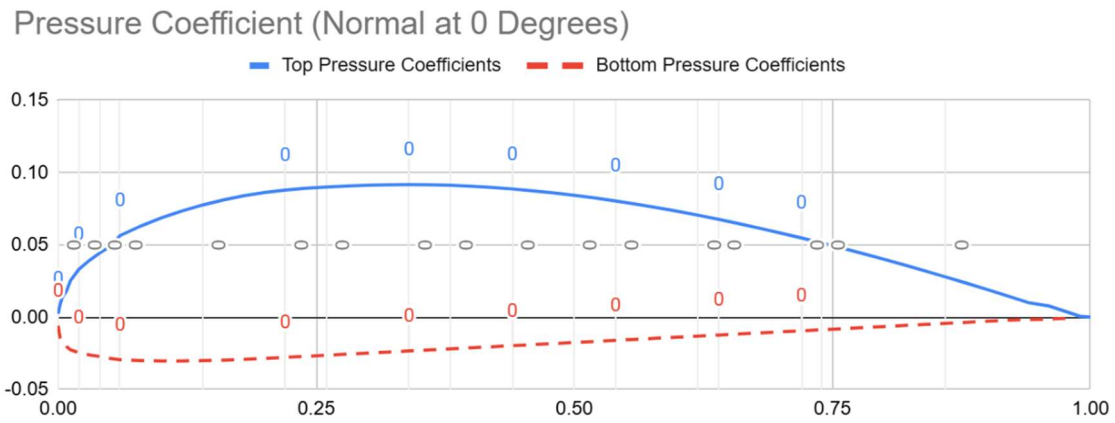

Figure 2: Pressure coefficient distribution normal to the chord for angle of attack 0°.

For pressure distribution normal and parallel to the chord at several angles of attack illustrated in Figures 2 through 11, Equations 4.2.1 and 4.2.2 are derived to provide valuable insight into the aerodynamic performance of the Clark Y-14 airfoil. Through pressure force measurements, the lift and drag calculations reveal an airfoil profile with angle of attack changes. Uncertainty in lift and drag coefficients from pressure force measurements exist from calibration errors of the pressure transducer or inaccurate pressure placement. Other uncertainties when collecting data include the accuracy of the hot-wire anemometer and the consistency of velocity measurements at different points in the wake.

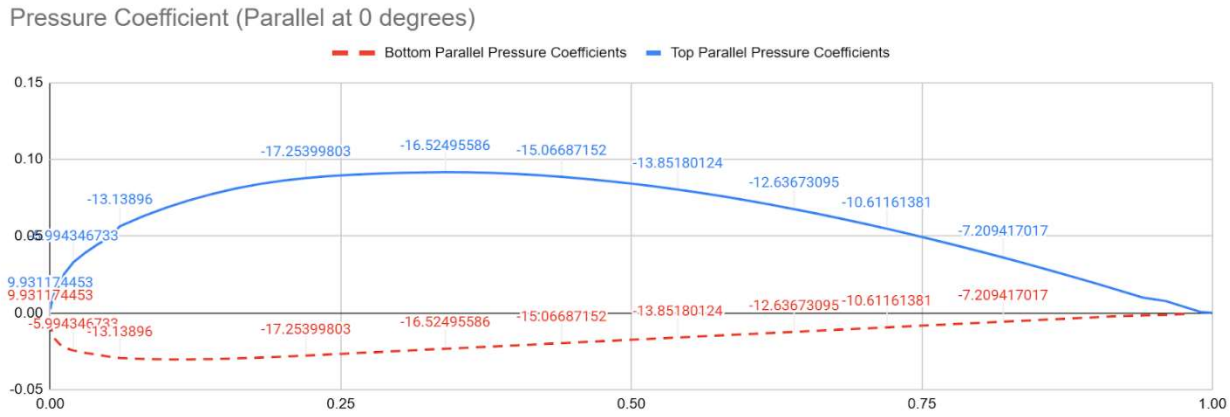

Figure 3: Pressure coefficient distribution parallel to the chord for angle of attack 0°.

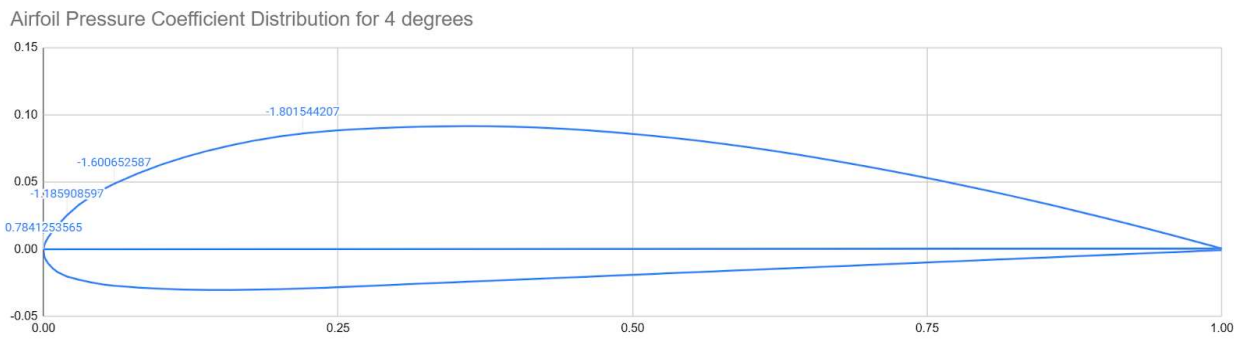

Figure 4: Pressure coefficient distribution of x-y locations on the airfoil surface for angle of attack 4°.

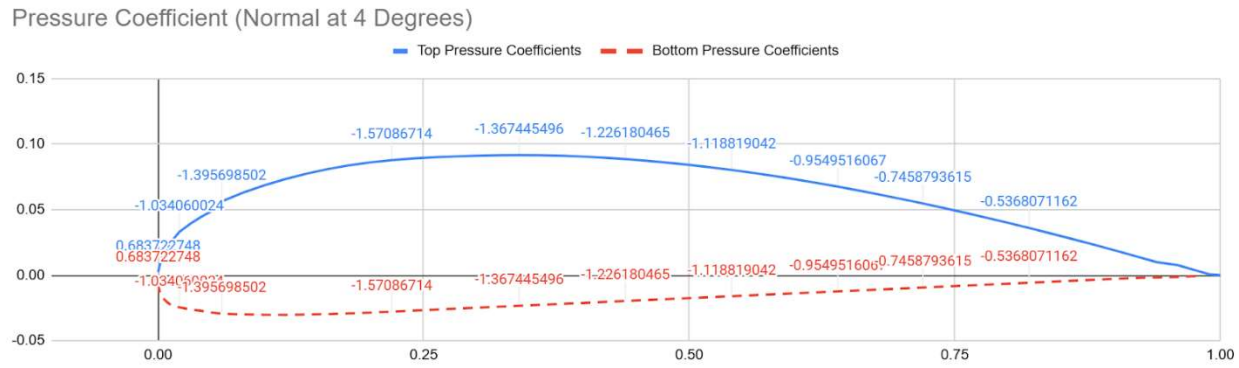

Figure 5: Pressure coefficient distribution normal to the chord for angle of attack 4°.

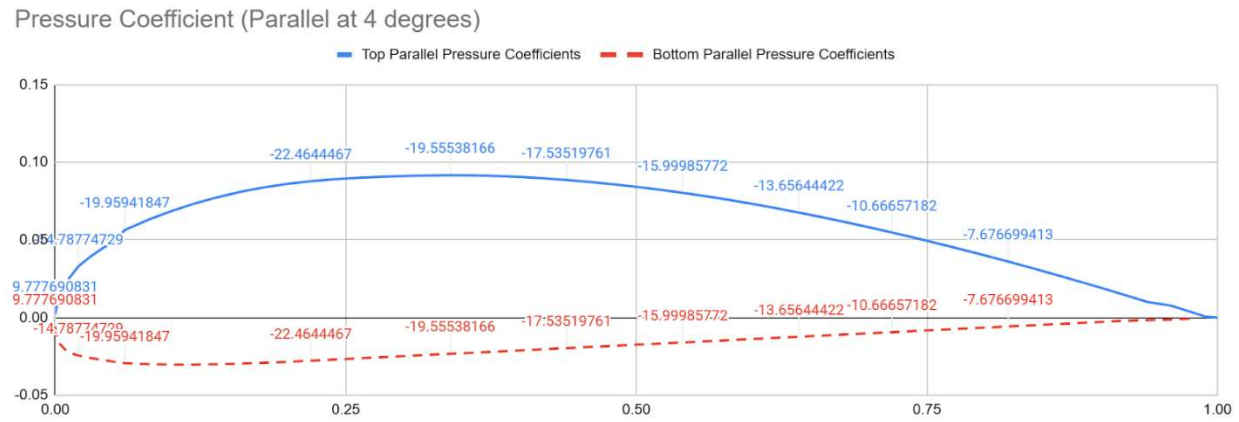

Figure 6: Pressure coefficient distribution parallel to the chord for angle of attack 4°.

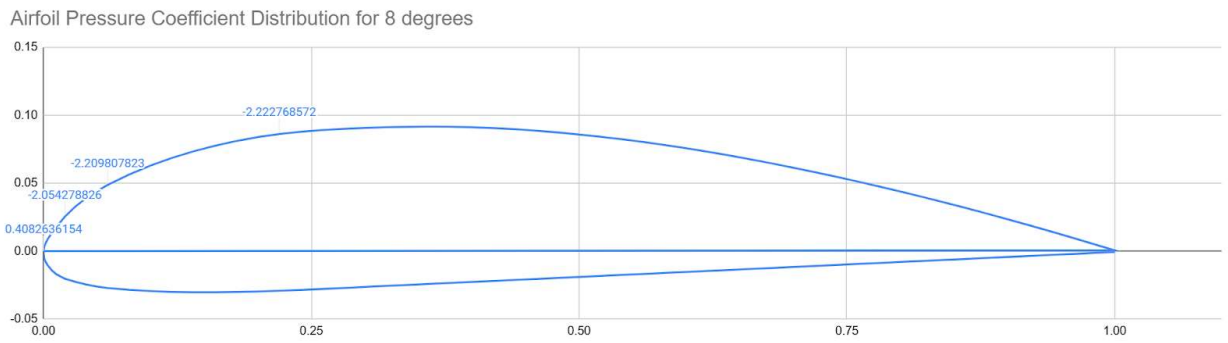

Figure 7: Pressure coefficient distribution of x-y locations on the airfoil surface for angle of attack 8°.

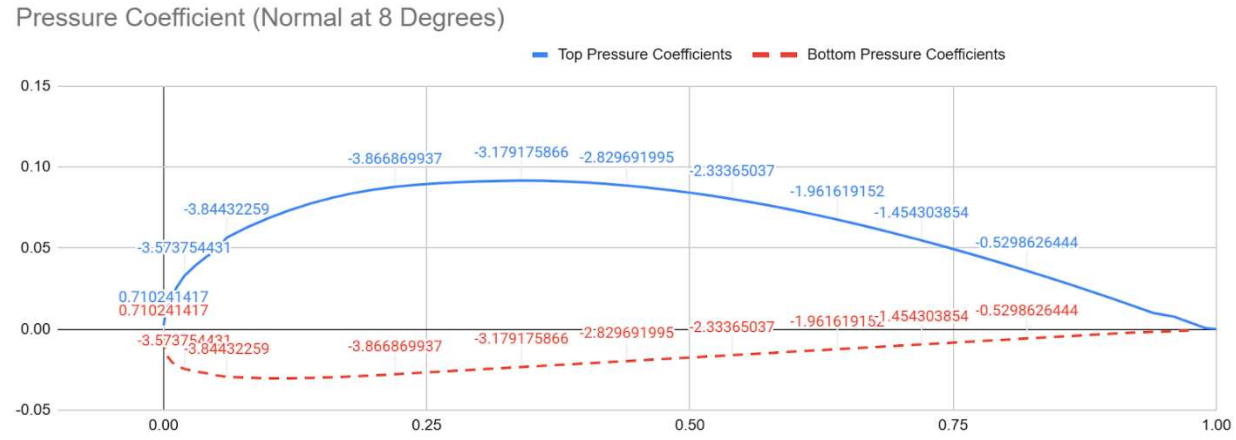

Figure 8: Pressure coefficient distribution normal to the chord for angle of attack 8°.

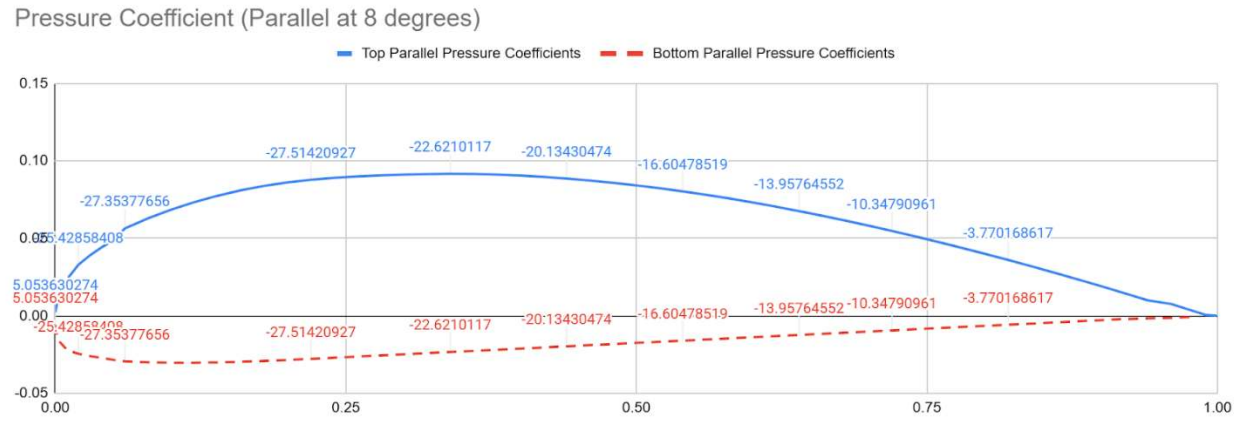

Figure 9: Pressure coefficient distribution parallel to the chord for angle of attack 8°.

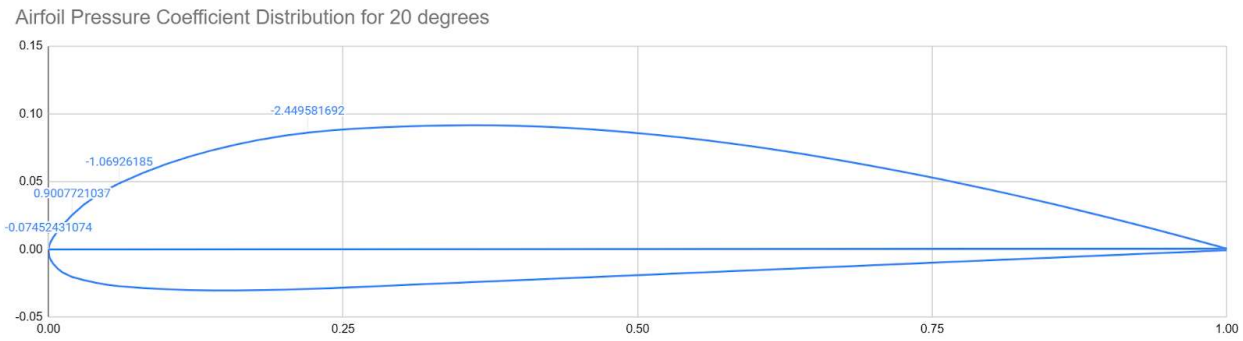

Figure 10: Pressure coefficient distribution of x-y locations on the airfoil surface for angle of attack 20°.

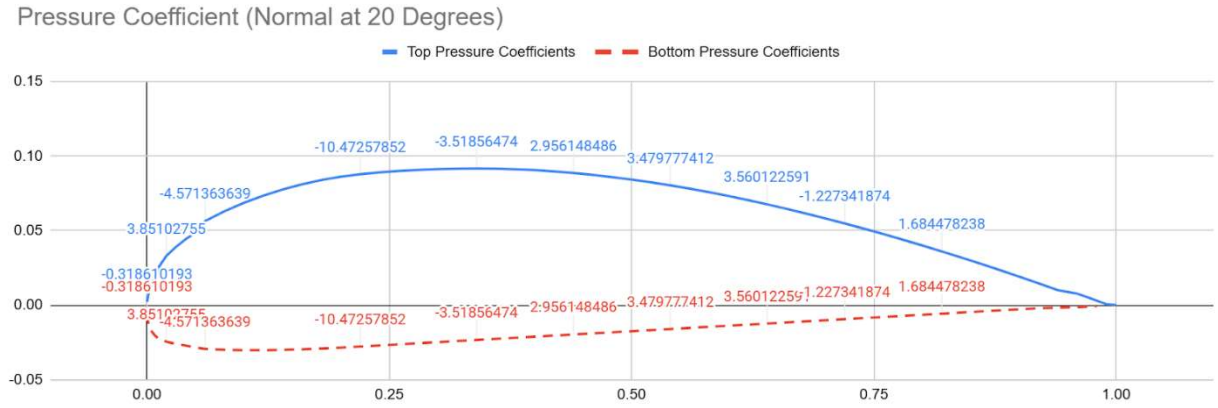

Figure 11: Pressure coefficient distribution normal to the chord for angle of attack 20°.

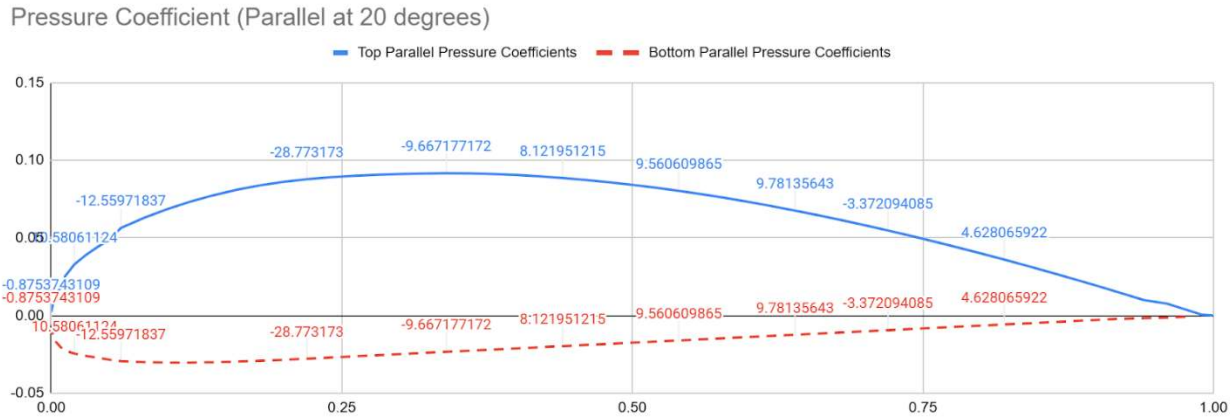

Figure 12: Pressure coefficient distribution parallel to the chord for angle of attack 20°.

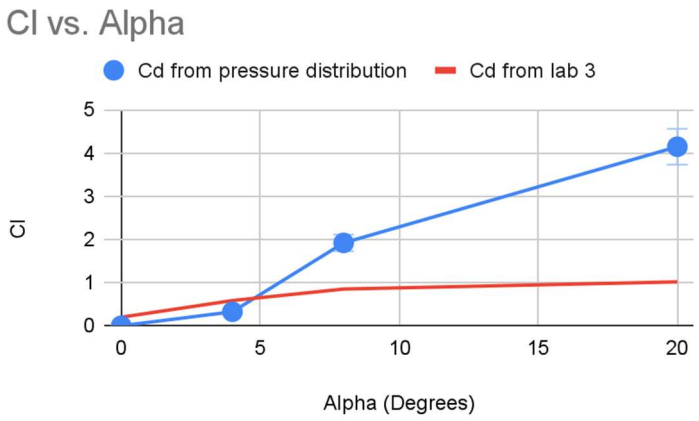

Figure 13: Lift and drag coefficient versus angles of attack 0, 4, 8, and 20°.

In this trend for Figure 13, coefficient of Lift versus angles of attack, the pressure forces derived from Equation 4.2.1 provides an understanding of drag increase by increasing the angle of attack. The trend in CL reflects the changes in pressure forces for both normal and tangential to the chord.

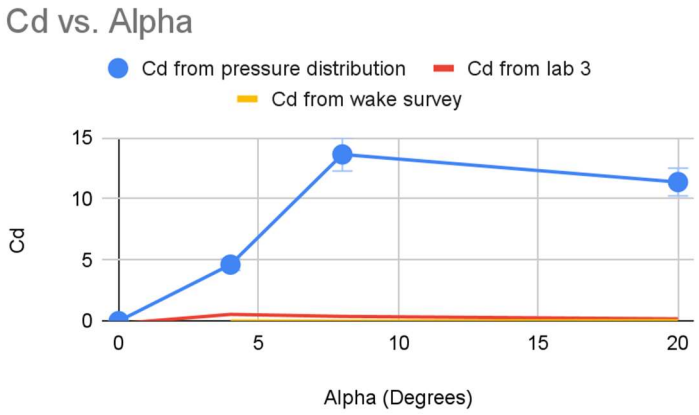

Figure 14: A Wake downstream survey by plotting drag coefficient versus angles of attack 0, 4, 8, and 20°.

The drag coefficient and drag force derived from Equation 4.2.2 and illustrated in Figure 14, increases sharply at higher angles of attack, demonstrating a typical behavior of airfoils approaching stall.

7. Conclusion

This experiment successfully characterized the aerodynamic performance of the Clark Y-14 airfoil through both pressure distribution measurements and wake survey techniques. By testing the airfoil at different angles of attack, we were able to compute the lift and drag coefficients for both clean and modified configurations, including the addition of slats and flaps. The results confirmed that the lift coefficient increased with the angle of attack, and the drag coefficient sharply rose as the airfoil approached stall conditions at 16°. These findings underscore the importance of both pressure and wake survey techniques in evaluating airfoil performance and provide valuable insights into the interaction between lift, drag, and stall characteristics.

The wake survey method proved to be an effective complementary tool for estimating drag, offering a less intrusive alternative to direct force measurements. The results also demonstrated the significant effect of slats and flaps on improving lift, particularly at higher angles of attack, while also highlighting the tradeoff between increased lift and the associated increase in drag.

The experimental findings contribute to a better understanding of how slats and flaps can be used to optimize airfoil performance under varying flight conditions. This study lays the foundation for future research aimed at further refining airfoil design and enhancing aerodynamic efficiency.

8. Acknowledgments

We want to thank Professor Sherif Hassaan for his guidance and instruction, which provided a solid theoretical foundation for understanding the purpose and scope of this experiment. We would also like to thank Teaching Assistant Cody Gonzalez for his assistance during the experiment, helping ensure that the procedures were conducted smoothly and accurately.

9. References

[1] MAE 108 Laboratory Manual

[2] Santos, Luciano Amaury dos. Drag Estimation by Wake Survey Performed Measuring Velocities and Measuring Total and Static Pressures. Proceedings of the 11th Brazilian Congress of Thermal Sciences and Engineering. [Online]. Retrieved from: https://abcm.org.br/anais/encit/2006/arquivos/Experimental%20Methods%20and%20Metrology/CIT06-0246.pdf (Accessed: 24 November 2024).

10. Appendices:

Appendix 1: Sample computations

This section will include sample computations that were done to reduce the data down to the final results.

Pressure force's normal and tangential components relative to the chord line

$$\text{Reading in meters} = \frac{\text{Anemometer reading (inH20)}}{39.37}$$

$$\text{Reading in Pascals} = \text{Reading in meters} * 9806.65$$

$$C_p = \frac{\text{Reading in Pascals}}{\frac{1}{2}\rho V^2}$$

$$F_{P,N} = \text{Reading in Pascals} * \sin\alpha$$

$$F_{P,C} = \text{Reading in Pascals} * \cos\alpha$$

Lift and Drag Forces

$$L = F_{P,N}\cos\alpha - F_{P,C}\sin\alpha$$

$$D = F_{P,C}\cos\alpha + F_{P,N}\sin\alpha$$

Lift and Drag Forces Coefficients

$$C_L = \frac{L}{q S_{REF}}$$

$$C_D = \frac{D}{q S_{REF}}$$

Drag Forces from Wave Survey

$$D = \sum 2 \times S \times \rho \times V_\infty^2 \times y_i - 2 \times S \times \rho \times V^2 \times y_{i+1}$$

Appendix 2: Experimental data

The following chart shows recorded data from the experiment.

Table 1: Pressure Force Measurement at α = 0°

Position	Anemometer Reading (inH20)	Reading in Meters	Reading in Pascals	Coefficient of Pressure	Normal	Parallel
Point 1	1.23	0.03	305.38	0.79	0.00	305.38
Point 2	-0.74	-0.02	-184.33	-0.48	0.00	-184.33
Point 3	-1.62	-0.04	-404.02	-1.05	0.00	-404.02
Point 4	-2.13	-0.05	-530.56	-1.38	0.00	-530.56
Point 5	-2.04	-0.05	-508.14	-1.32	0.00	-508.14
Point 6	-1.86	-0.05	-463.31	-1.21	0.00	-463.31
Point 7	-1.71	-0.04	-425.94	-1.11	0.00	-425.94
Point 8	-1.56	-0.04	-388.58	-1.01	0.00	-388.58
Point 9	-1.31	-0.03	-326.31	-0.85	0.00	-326.31
Point 10	-0.89	-0.02	-221.69	-0.58	0.00	-221.69
Point 11	-1.24	-0.03	-308.87	-0.80	0.00	-308.87
Point 12	-1.41	-0.04	-351.22	-0.91	0.00	-351.22
Point 13	-1.76	-0.04	-438.40	-1.14	0.00	-438.40
Point 14	-1.66	-0.04	-413.49	-1.08	0.00	-413.49
Point 15	-0.61	-0.02	-151.94	-0.40	0.00	-151.94
Point 16*	1.48	0.04	368.65	0.96	0.00	368.65
Point 17	-0.57	-0.01	-141.98	-0.37	0.00	-141.98
Point 18	-0.55	-0.01	-137.00	-0.36	0.00	-137.00

Table 2: Pressure Force Measurement at α = 4°

Position	Anemometer Reading (inH20)	Reading in Meters	Reading in Pascals	Coefficient of Pressure	Normal	Parallel
Point 1	1.21	0.03	301.40	0.78	21.02	300.66
Point 2	-1.83	-0.05	-455.83	-1.19	-31.80	-454.72
Point 3	-2.47	-0.06	-615.25	-1.60	-42.92	-613.75
Point 4	-2.78	-0.07	-692.47	-1.80	-48.30	-690.78
Point 5	-2.42	-0.06	-602.80	-1.57	-42.05	-601.33
Point 6	-2.17	-0.06	-540.52	-1.41	-37.71	-539.21
Point 7	-1.98	-0.05	-493.20	-1.28	-34.40	-492.00
Point 8	-1.69	-0.04	-420.96	-1.10	-29.36	-419.94
Point 9	-1.32	-0.03	-328.80	-0.86	-22.94	-328.00
Point 10	-0.95	-0.02	-236.63	-0.62	-16.51	-236.06
Point 11	-0.26	-0.01	-64.76	-0.17	-4.52	-64.61
Point 12	-0.76	-0.02	-189.31	-0.49	-13.21	-188.85
Point 13	-0.41	-0.01	-102.13	-0.27	-7.12	-101.88
Point 14	-0.42	-0.01	-104.62	-0.27	-7.30	-104.36
Point 15	-0.43	-0.01	-107.11	-0.28	-7.47	-106.85
Point 16*	1.47	0.04	366.16	0.95	25.54	365.27
Point 17	-0.43	-0.01	-107.11	-0.28	-7.47	-106.85
Point 18	-0.45	-0.01	-112.09	-0.29	-7.82	-111.82

Table 3: Pressure Force Measurement at α = 8°

Position	Anemometer Reading (inH20)	Reading in Meters	Reading in Pascals	Coefficient of Pressure	Normal	Parallel
Point 1	0.63	0.02	156.93	0.41	21.84	155.40
Point 2	-3.17	-0.08	-789.61	-2.05	-109.89	-781.93
Point 3	-3.41	-0.09	-849.39	-2.21	-118.21	-841.13
Point 4	-3.43	-0.09	-854.38	-2.22	-118.91	-846.06
Point 5	-2.82	-0.07	-702.43	-1.83	-97.76	-695.60
Point 6	-2.51	-0.06	-625.21	-1.63	-87.01	-619.13
Point 7	-2.07	-0.05	-515.62	-1.34	-71.76	-510.60
Point 8	-1.74	-0.04	-433.42	-1.13	-60.32	-429.20
Point 9	-1.29	-0.03	-321.33	-0.84	-44.72	-318.20
Point 10	-0.47	-0.01	-117.07	-0.30	-16.29	-115.93
Point 11	0.81	0.02	201.76	0.52	28.08	199.80
Point 12	0.06	0.00	14.95	0.04	2.08	14.80
Point 13	0.60	0.02	149.95	0.39	20.87	148.49
Point 14	0.90	0.02	224.18	0.58	31.20	222.00
Point 15	-0.24	-0.01	-59.78	-0.16	-8.32	-59.20
Point 16*	1.48	0.04	368.65	0.96	51.31	365.06
Point 17	-0.03	0.00	-7.47	-0.02	-1.04	-7.40
Point 18	-0.15	0.00	-37.36	-0.10	-5.20	-37.00

Table 4: Pressure Force Measurement at α = 20°

Position	Anemometer Reading (inH20)	Reading in Meters	Reading in Pascals	Coefficient of Pressure	Normal	Parallel
Point 1	-0.12	0.00	-28.65	-0.07	-9.80	-26.92
Point 2	1.39	0.04	346.23	0.90	118.42	325.35
Point 3	-1.65	-0.04	-411.00	-1.07	-140.57	-386.21
Point 4	-3.78	-0.10	-941.56	-2.45	-322.03	-884.78
Point 5	-1.27	-0.03	-316.34	-0.82	-108.20	-297.27
Point 6	1.07	0.03	265.78	0.69	90.90	249.75
Point 7	1.26	0.03	312.86	0.81	107.00	293.99
Point 8	1.29	0.03	320.08	0.83	109.47	300.78
Point 9	-0.44	-0.01	-110.35	-0.29	-37.74	-103.69
Point 10	0.61	0.02	151.45	0.39	51.80	142.31
Point 11	1.45	0.04	360.18	0.94	123.19	338.46
Point 12	1.38	0.04	343.74	0.89	117.57	323.01
Point 13	0.86	0.02	214.96	0.56	73.52	202.00
Point 14	0.40	0.01	99.88	0.26	34.16	93.86
Point 15	0.55	0.01	136.00	0.35	46.52	127.80
Point 16*	1.47	0.04	364.92	0.95	124.81	342.91
Point 17	1.31	0.03	326.81	0.85	111.77	307.10
Point 18	0.80	0.02	200.02	0.52	68.41	187.96

Table 5: Calibration of Hot Film

Velocity from Pitot Tube (m/s) (V)	Voltage Value (E)	Standard Deviation of Voltage
5.069	3.1053	0.00259976
6.938	3.25439	0.00288823
9.036	3.40787	0.00395683
12.05	3.56266	0.00324157
15.02	3.69331	0.0035872
20.06	3.88358	0.00439787
25.69	4.07724	0.00548864
30.03	4.21875	0.00525716
35.31	4.36941	0.004815

Table 6: Inlet Velocity profile

Velocity from Pitot Tube (m/s)	Distance from the Wall (mm)
23.76	76
23.71	106
23.58	136
23.6	166
23.58	196
23.73	226
23.67	256

Table 7: Wake Measurement at α = 0°

Voltage Values	Distance (mm)	Voltage Values	Distance (mm)
3.95652	0	3.98785	2.016
3.9375	-1.003	3.99828	2.567
3.9374	-1.512	4.00217	3.015
3.9326	-2.081	4.00732	4.067
3.93343	-3.016	4.01027	5.046
3.95295	-4.002	4.01837	15.481
3.98095	-5.006		
4.00034	-6.008		
4.01221	-7.022		
4.00897	-8.007		
4.00858	-9.007		
4.01004	-15.006		
3.92623	-2.51		
3.94186	-0.501		
3.95981	0.555		
3.96939	1.066		
3.98068	1.524		

Table 8: Wake Measurement at α = 4°

Voltage Values	Distance (mm)	Voltage Values	Distance (mm)
3.99847	0	3.99588	-9.048
3.98708	-0.5	3.99679	-9.506
3.98092	-1.046	4.00795	-11.076
3.95982	-1.495	4.01094	-12.027
3.94765	-2.034	4.00564	-13.006
3.93968	-2.546	3.9911	1.009
3.93278	-3.047	3.9958	2.07
3.91973	-3.515	3.99456	3.039
3.90985	-4.067	3.99412	4.089
3.90501	-4.527	3.99673	5.197
3.8987	-5.06	3.99753	8.03
3.90308	-5.525	4.00876	12.359
3.91033	-6.009	4.01209	15.22
3.92072	-6.554		
3.92936	-7.012		
3.95388	-7.577		
3.97205	-8.04		
3.98332	-8.506		

Table 9: Wake Measurement at α = 8°

Voltage Values	Distance (mm)	Voltage Values	Distance (mm)
4.01913	-30.519	4.00984	0
4.01916	-25.107	4.00634	1.005
4.01497	-20.124	4.00702	2.177
4.01382	-15.015	4.01351	3.151
4.00656	-13.078	4.01192	8.215
4.00683	-12.18	4.01627	15.14
3.98435	-11.027	4.02161	20.321
3.94974	-10.094	4.02422	25.003
3.90661	-9.001	4.02878	30.035
3.87857	-8.013	3.88899	-5.558
3.86941	-6.999	3.87177	-6.581
3.88135	-6.018	3.87292	-7.459
3.90631	-5.043	3.91618	-4.497
3.93346	-4.053	3.94575	-3.505
3.96076	-3.09		
3.99	-2.069		
4.00233	-1.001		

Table 10: Wake Measurement at α = 20°

Voltage Values	Distance (mm)	Voltage Values	Distance (mm)	Voltage Values	Distance (mm)
4.09475	-50.415	3.51866	9.003	3.85919	-2.006
4.09347	-44.981	3.50372	10.019	3.83678	-1.045
4.09306	-40.459	3.48717	11.017	3.79305	0.001
4.09151	-34.654	3.48584	12.163	3.7572	1.005
4.08213	-25.641	3.48052	13.131	3.71555	2.047
4.08595	-23.555	3.48395	14.22	3.68856	3.068
4.07705	-18.59	3.49077	15.136	3.64945	4.074
4.07281	-17.477	3.49584	16.023	3.61363	5.068
4.05268	-14.108	3.50947	17.208	3.57955	6.099
4.04577	-13.004	3.51171	18.126	3.55187	7.053
4.0421	-11.999	3.53423	19.265	3.52455	8.007
4.03246	-11.061	3.56151	20.262	3.51866	9.003
4.03013	-10.148	3.59667	22.208	3.91173	32.905
4.00926	-9.031	3.62377	23.453	3.93754	34.249
3.99286	-8.016	3.66112	25.091	3.98417	36.409
3.98268	-7.018	3.7009	26.393	4.00959	37.278
3.95639	-6.079	3.74007	27.655	4.04871	38.574
3.94204	-5.012	3.77739	29.029	4.05959	40.017
3.91786	-4.014	3.82336	30.172	4.09	41.674
3.89141	-3.017	3.86498	31.485	4.11544	45.016